Modelling of embolus transport and embolic stroke

I. D. Šutalo[1,2], A. Bui[3], K. Liffman[1,2] & R. Manasseh[4,5]
[1]*Materials Science and Engineering, Commonwealth Scientific and Industrial Research Organisation (CSIRO), Australia*
[2]*Curtin Health Innovation Research Institute, Curtin University, Australia*
[3]*Idaho National Laboratory, USA*
[4]*Faculty of Engineering and Industrial Sciences, Swinburne University of Technology, Australia*
[5]*Mechanical Engineering, The University of Melbourne, Australia*

Abstract

Cerebral microembolism may lead to the restriction of blood supply due to damaged blood vessel tissue (focal ischemia) which is increasingly seen as the cause of cognitive deterioration including Alzheimer's disease and vascular dementia. The flow through fractal models of the peripheral vasculature of the Anterior Cerebral Arteries (ACA) and Middle Cerebral Arteries (MCA) was modelled. The multi-scale model of the cerebral vasculature was coupled with blood flow and embolus transport models. The model incorporated asymmetric bifurcation trees, embolus-vascular interactions and autoregulation. Simulations were carried out where the embolus deposition rate, embolus diameter and embolus introduction rate were varied. Increasing the embolus diameter and embolus introduction rate increased the number of blocked terminal arteries to a quasi steady-state. For a low embolus deposition rate the MCA and ACA territory had the same embolization dynamics, even though, the MCA was larger than the ACA. It was also found for a higher embolus deposition rate the MCA, due to its more expansive structure, was less prone to occlusion than the ACA. The results also showed the effect of a single blockage is expected to be less severe in asymmetric flow than symmetric flow. This model will assist in developing a better understanding into embolic stroke and effect of

WIT Transactions on Biomedicine and Health, Vol 15, © 2011 WIT Press
www.witpress.com, ISSN 1743-3525 (on-line)
doi:10.2495/EHR110301

microembolism and on the alteration of blood flow distribution in the circle of Willis.
Keywords: embolic stroke, microembolism, cerebral arteries, cerebral hemodynamics, ischemia, numerical models.

1 Introduction

Cerebral microembolism and microinfarction may be the reason for gradual degradation of brain functionality and cognitive impairment [1], including Alzheimer's disease (AD) and vascular dementia [2]. Microembolism has been investigated clinically [3], in animals [4, 5] and analytically [6, 7]. Chung *et al.* [7] established the mechanisms of embolic stroke and studied the relationship between embolic stroke and cerebral blood flow. The effects of embolus dissolution and interaction with a vascular bifurcating network were incorporated in a probabilistic Monte Carlo framework for embolic stroke prediction. However, they employed simplified fluid dynamics and cerebral vasculature models without taking into consideration the effect of autoregulation. Hague and Chung [8] subsequently carried out a basic fluid dynamics analysis of the vascular tree to justify their flow weighting scheme. They used symmetric bifurcations whereas they are usually asymmetric [7, 8].

Niimi *et al.* [6] modelled a small portion of a realistic cerebral microcirculation network and included an autoregulation mechanism based on wall shear variation. Variation of blood flow in the circle of Willis (CoW) during focal ischemia caused by occlusion of the MCA was examined in the numerical simulation by Hudetz *et al.* [9]. However, details of the flow in the arterial networks beyond the CoW were not considered. More advanced three-dimensional (3D) modelling studies have modelled flow and deformation of red blood cells in microvessels [10, 11].

The present study simulates flow and embolus transport through fractal models of the peripheral vasculature of the ACA and MCA to investigate the effect of embolus deposition rate, diameter and introduction rate on the percentage of blocked terminal arteries. This model is novel in that it combines models of cerebral vascular networks and the flows inside [12], with a statistical model of microembolic occlusion which includes embolus transport by blood flow and embolus-vasculature interactions, asymmetric bifurcation trees and autoregulation.

1.1 Fluid dynamics of embolus transport and cerebral microembolism

The transport of emboli in the cerebral microcirculatory system is mainly governed by the cerebral vasculature geometry, the blood flow characteristics, and the interactions of the emboli with the vascular system. These factors are interrelated and influenced by physiological and pathological variations and mechanisms including cerebral blood flow, autoregulation, metabolism, and ageing. Experimental observations have identified that the dominant geometry of the cerebral blood vessels with diameters larger than that of the capillaries

(approximately $10\,\mu$m) is the fractal tree-like structure with bifurcations dominating [13, 14]. The embolus-bifurcation interaction is a very important factor in the embolus transport in the cerebral vasculature.

The cerebral blood flow transporting the emboli is governed by the systemic pressure, vascular geometry, blood rheology and autoregulation. The Reynolds number in the cerebral microcirculation network is 10^{-1}-10^{-3} [15] so the blood flow rate, Q, can be defined by Poiseuille's law:

$$Q = -\frac{\pi D_{vessel}^{4}}{128\,\mu}\frac{\partial P}{\partial l} \tag{1}$$

The transport of emboli in the cerebral vasculature is a dynamic process with the emboli changing and sustaining various interactions while moving along the branching vascular network. The emboli can dissolve [16], interact with the blood vessel wall [17] or vascular network bifurcations [18]. These interactions are the most important factor which may lead to the narrowing of vascular lumen and possible blood vessel occlusion and brain infarction. Alzheimer's patients have deposits of Amyloid Beta (Aβ) which is a vasoconstrictor. The clinical study by Bateman *et al.* [19] found significant reduction of blood flow (as much as 18%) in AD patients and increase of flow resistance (up to 23%), which can be explained by both the effects of Aβ vasoconstriction [20] and partial blockage of large number of arterioles by microemboli.

2 Methods

2.1 Cerebral vasculature and flow models

Using the fractal scaling concept, a branching tree model, which possesses physiologically meaningful morphology, can be created for the treelike part of the cerebral vasculature. In this work, a three-dimensional (3D) branching-tree model of cerebral vasculature has been constructed using the Constrained Constructive Optimization method (CCO) [21].

A model of pulsatile flow and pressure distribution in a vascular branching network which takes into consideration the effect of variable blood rheology and blood vessel compliance has been developed by Bui *et al.* [12]. They showed the flow and pressure distributions in a complex vascular branching network can be described by a system of differential algebraic equations (DAEs) representing the mass conservation at the branching points. For human cerebral blood vessel characteristics, this system of DAEs is generally stiff and can be solved by using the MATLAB or other stiff differential equation solvers. Following the work by Pries *et al.* [22], the blood viscosity is made a function of the vessel diameter and hematocrit level. The effect of Aβ vasoconstriction on certain sections of the cerebral circulatory system is simulated by varying the diameter of the branches in the affected area, which leads to the localized increase of flow resistance defined as:

$$R = \frac{128\,\mu L_{vessel}}{\pi D_{vessel}^{4}}\,. \tag{2}$$

2.2 Blood flow autoregulation

Autoregulation plays a very important role in maintaining constant supply of oxygen and other metabolic ingredients to the brain and maintaining constant blood flow in the capillary networks [23]. Consequently, the deterioration of neurovascular autoregulation can have a disruptive effect on cerebral blood flow, leading to brain dysfunction and potentially AD [24]. A few recent studies have coupled autoregulation and hemodynamic models at microcirculation level [22]. In the present work, the cerebral blood flow autoregulation was modelled through a vasodilation/vasoconstriction feedback in response to the change of wall shear stress, and was correlated to the relative blood vessel diameter [6].

2.3 Embolus transport and interaction models

The model of material transport developed in this work has been based on the detailed solution of pressure and flow distributions obtained for all components of the vascular branching tree. Inside a segment of a vascular branching tree model without diffusion, the mass transport of material is described by the Reynolds Transport Theorem:

$$\frac{d\left(\bar{c}V\right)}{d\mathrm{t}} = Q_{in}c_{in} - Q_{out}c_{out} + \dot{m}_c \tag{3}$$

where $\bar{c}$ is the average concentration of material, Q the volume flow rate, V the segment volume, c the concentration and $\dot{m}_c$ is the generation/loss rate of material.

Generally, the material concentration varies along the segment length and a species transport model should take this into consideration [25, 26]. As a first approximation, the average concentration in the segment was assumed to be an average of material concentrations at the inlet and outlet of the segment, i.e.

$$\bar{c} = \frac{1}{2}\left(c_{in} + c_{out}\right) \tag{4}$$

Since the change of the segment volume can be described as:

$$\frac{dV}{d\mathrm{t}} = Q_{in} - Q_{out} \tag{5}$$

a mass conservation of the material can be derived from eqn. (3) as follows:

$$V\frac{d\left(c_{in} + c_{out}\right)}{d\mathrm{t}} = \left(Q_{in} + Q_{out}\right)\left(c_{in} - c_{out}\right) + 2\dot{m}_c \tag{6}$$

Eqn (6) has a form similar to the oxygen transport formulation given by Boas *et al.* [27]. Red blood cells with microvascular bifurcations can lead to a phase separation with subsequent variation of hematocrit level in the branches of different sizes. This phenomenon was termed as Fahraeus-Lindqvist (or plasma skimming) effect [28]. This effect can also explain the selective propagation of microemboli in the cerebral vascular network which may have a big implication for cerebral embolism [18].

At a bifurcation point shown in Fig. 1, the conservations of overall flow and embolus concentration dictate:

$$Q_o = Q_1 + Q_2 \tag{7}$$

$$Q_o c_o = Q_1 c_1 + Q_2 c_2 \tag{8}$$

The variations of c_1 and c_2 relative to c_0 are caused by phase separation at the bifurcation point as described above. The relationship between ratios c_1/c_0 and c_2/c_0 and flow rates are derived from eqns. (7) and (8) as:

$$Q_1\left(1 - \frac{c_1}{c_0}\right) = -Q_2\left(1 - \frac{c_2}{c_0}\right) \tag{9}$$

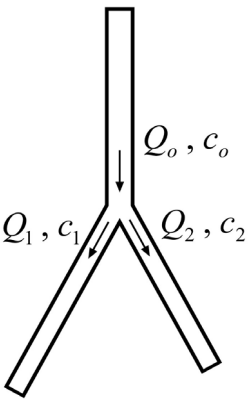

Figure 1: Flow and embolus concentration at a bifurcation point.

Experiments [18] conducted on microemboli with size ranging from 7 to 210 μm in an in-vitro flow system mimicking the human MCA, indicate that interactions of emboli of various sizes with microvascular bifurcations would lead to the preferential transport of the largest emboli along the main arterial trunks. Using these experimental data an empirical relationship between the relative concentration c_1/c_2 and branch size ratio D_1/D_2 can be correlated:

$$\frac{c_1}{c_2} = 1 - a\left(1 - \frac{D_1}{D_2}\right) \tag{10}$$

with $D_1 \le D_2$ and the inclination coefficient a is defined by $a = 0.05 + 0.1823\left(d_e - 7\right)$ where d_e is the embolus diameter in μm.

Eqns. (9) and (10) define the effect of embolus separation at the vascular branching points. The interaction of emboli and the blood vessel wall, while potentially being a factor leading to gradual reduction of the arterial lumen and subsequent blockage and ischemia, may also be a major mechanism of removing the emboli from the blood flow [17]. This interaction is dependent on the distribution of the embolic particles across the flow. Alevriadou and McIntire [17] showed the steady-state flux of embolus deposition has the form:

$$J(x) = c \Big/ \left[\frac{1}{k} + 1.48 \left(\frac{4U\Gamma^2}{Dx} \right)^{-1/3} \right] \tag{11}$$

where c denotes the bulk embolus concentration, k the adhesion rate constant, Γ the embolus diffusivity, and U the flow velocity in the axial direction *x*. The embolic deposition is therefore driven by two mechanisms, namely adhesion reaction and cross-flow diffusion, which are defined by adhesion rate constant and embolic diffusivity, respectively. The diffusion coefficient can also be determined in terms of the local shear rate as: $\Gamma \approx \gamma^n$, with n being a constant [17]. In this work, only the effect of adhesion was considered and the adhesion rate coefficient was assumed to be equal to that of either activated platelets ($k = 3.5 \times 10^{-3}$ m/s) or unactivated platelets ($k = 2.5 \times 10^{-6}$ m/s) [29].

Based on the flow and embolus distribution in the vascular network, an occlusion probability map is computed and used to initiate blockages in the network at a specified rate. Occlusion probability is assumed to depend not only on the relation between embolus size and the local blood vessel size, but also on the embolus distribution, which, in turn, is determined by the flow and embolus-vasculature interactions as described above. In addition, the occlusion probability is reduced with the increase of embolus residence time, i.e. occlusion should happen to the branches close to the root first. The presence of blockages in the vascular network will alter the flow and embolus distribution and affect further creation of blockages in the network. Therefore, the flow and embolus distributions are recalculated each time when a new blockage appears or an old one clears. In each simulation case, the computation has been conducted until a statistical balance of blockage creation and clearance is established in the system.

2.4 Cerebral vascular geometry

Fractal models of the peripheral vasculature of the ACA and MCA were constructed [12] and have approximately 1400 and 2800 terminal points, respectively, with the total number of segments equal to 2800 and 5600, respectively. A constant cerebral perfusion pressure of 62.8 mmHg (8367 Pa) was used. Only spherical solid emboli were considered with a constant dissolution rate of 0.1 mm per hour [7]. The rate of embolus introduction into the ACA and MCA peripheral vascular was a function of total flow rate under normal conditions (i.e., without occlusion), so that the embolus concentration was assumed to be similar at the inlets to the cerebral vascular territories.

3 Results and discussion

3.1 Factors affecting blood flow and embolus transport

Simulations were conducted on branching fractal models of the peripheral vasculature of the ACA and MCA. Among the factors affecting the blood flow and embolus transport it was predicted that embolus separation at branching

points and flow autoregulation have small effects on embolic occlusion and embolization dynamics. For the ACA peripheral vasculature the activation of autoregulation was seen to marginally reduce the vascular blockage (Fig. 2(a)) from emboli of similar sizes entering the system at a similar rate. The effect of embolus deposition rate, embolus diameter and embolus introduction rate were also investigated.

3.2 Effect of embolus deposition rate

Embolus deposition in arteries larger than the embolus size was predicted to have much larger influence on embolization. The increase of embolus deposition rate from $2.5x10^{-6}$ m/s to $3.5x10^{-3}$ m/s for ACA peripheral vasculature significantly decrease the number of emboli available to block smaller arterioles (Fig. 2(b)) and resulted in an approximately 36% reduction in vascular blockage.

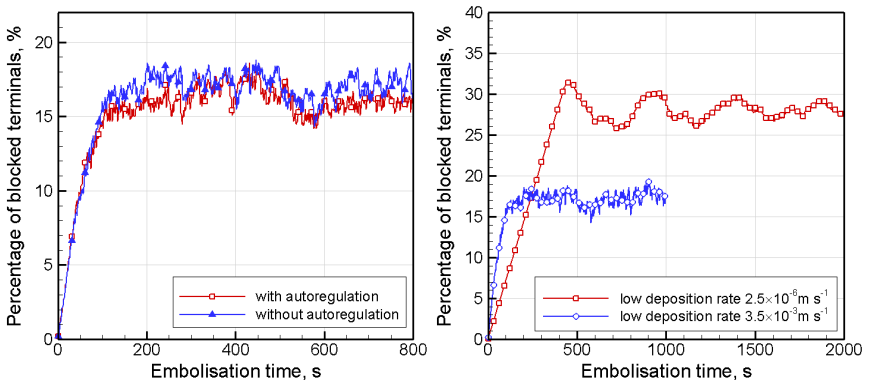

Figure 2: Effects of autoregulation and deposition rate on embolization on the ACA vasculature, 1 embolus per second.

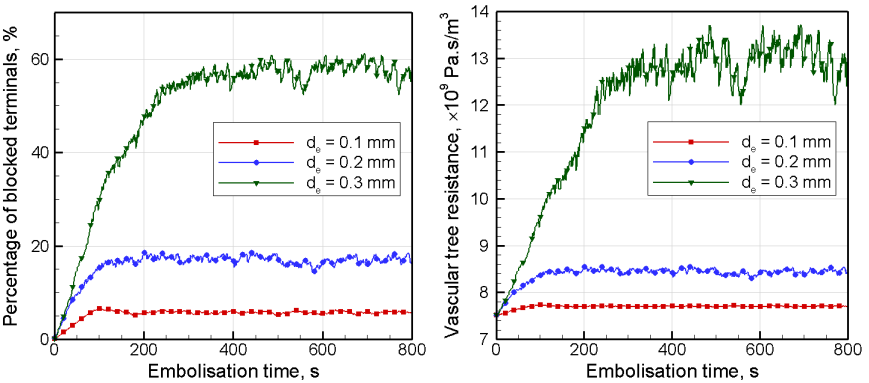

Figure 3: Percentage of blocked terminals and vascular tree resistance on the ACA vasculature, 1 embolus per second, deposition rate $3.5x10^{-3}$ m/s.

3.3 Effect of embolus diameter

Figure 3 shows the variations in time of the blocked terminal percentage and total vascular tree resistance. Similar to the investigation by Chung *et al.* [7], the portion of the blocked terminal arteries increases and reaches a quasi equilibrium state after a certain embolization time. Both this saturated blockage percentage and transition time were also found to be dependent on the embolus diameter (Fig. 3). Increase in embolus diameter from 0.2 to 0.3 mm increased the percentage of blocked terminals, so that embolus of 0.3 mm diameter had approximately three times higher percentage of blocked terminals compared to embolus of 0.2 mm. Chung *et al.* [7] also found that the percentage of blocked arteries increased with embolus diameter, especially for > 0.2 mm. The increase in embolus diameter also increased the vascular resistance which restricts blood flow and may lead to focal ischemia.

3.4 Effect of embolus introduction rate

Increase in embolus introduction rate from 0.5 to 3 embolus per second increased the number of blocked terminals fourfold (as shown in Fig. 4), to 40% at a embolus introduction rate of 3 embolus per second. Chung *et al.* [7] also found that increased embolus rate also increased the danger of blockage.

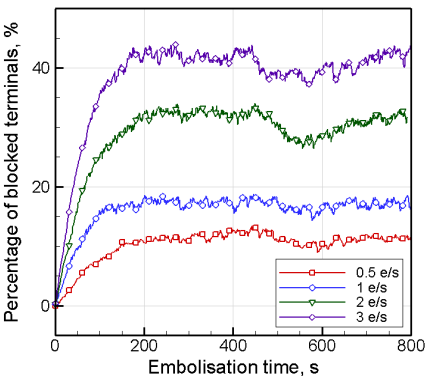

Figure 4: Effect of embolus introduction rate on embolization of the ACA vasculature, d_e = 0.2 mm, deposition rate 3.5×10^{-3} m/s.

3.5 MCA versus ACA cerebral vascular territory

Although the MCA territory is significantly larger than the ACA territory and the blood flow rates in them are different, they were predicted to have identical embolization dynamics, when emboli of similar size and concentration were introduced into the circulatory systems and a low embolus deposition rate of 2.5×10^{-6} m/s was assumed (Fig. 5). However, with a higher embolus deposition rate of 3.5×10^{-3} m/s, the MCA, due to its more expansive structure, had lower percentage of blocked terminals for a given embolus diameter. Hence, the MCA seemed to be less prone to occlusion and focal ischemia than the ACA (compare Fig. 3 and Fig. 6).

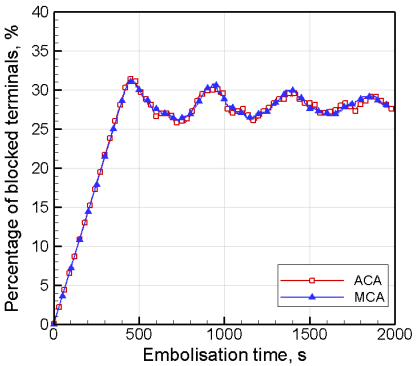

Figure 5: Embolization in ACA and MCA vasculature at low embolus deposition rate - d_e = 0.2 mm, deposition rate = 2.5x10^{-6} m/s.

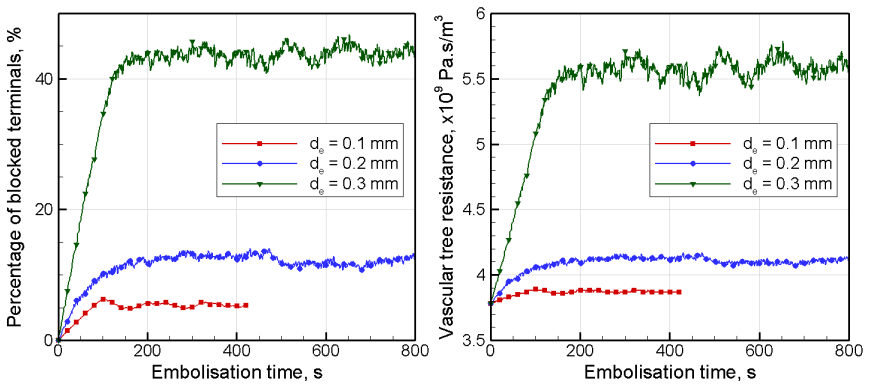

Figure 6: Percentage of blocked terminals and vascular tree resistance on the MCA vasculature, embolus introduction rate equivalent to 1 embolus per second in ACA, deposition rate 0.0035 m/s.

3.6 Effect of asymmetric versus symmetric bifurcations

Our model is different from the models by Chung *et al.* [7] and Hague and Chung [8] in that asymmetric bifurcation trees are considered rather than just symmetric. For a similar number of terminals, an asymmetric vascular branching tree will have more bifurcation levels compared to a symmetric one. The effect of a single blockage is therefore expected to be less severe in asymmetric flow system. Due to the effect of preferential transport of large emboli in the large vascular branch they have more opportunity to absorb before blocking terminals.

3.7 Current model and future model improvements

The current numerical model, which incorporates human cerebral vascular morphology, hemodynamics, blood flow autoregulation, physics of embolus

transport and interactions. It can assist in developing a better understanding into embolic stroke and effect of microembolism and associated focal ischemia on the alteration of blood flow distribution and increased resistance in the CoW. The model can also be used make comparisons with in-silico experiments.

Wijman *et al.* [30] showed that cerebral infarcts occurred more frequently in the MCA than the ACA main arteries. In future, the inlet embolus concentration at the inlet of the peripheral vasculature can be varied when comparing the ACA and MCA territory blockage.

Previously, Šutalo *et al.* [31] modelled the blood flow in a coupled computational fluid dynamics (CFD) model of the 3D patient-specific CoW and branching tree fractal model of the cerebral vascular networks [32]. In future, it is possible to couple this model of the embolus transport in peripheral cerebral vascular networks with embolus transport in the CoW. Such a coupled model of the embolus transport in the CoW and cerebral vasculature could be used to compare with experimental results by Chung *et al.* [33] from a patient-specific silicone model of the CoW showed the embolus trajectory through the cerebral arteries is dependent on embolus size and favours the MCA for large emboli (≥ 0.5 mm).

4 Conclusion

The blood flow and embolus transport through fractal models of the peripheral vasculature of the ACA and MCA were modelled to investigate the effect of embolus variables on the embolization of the terminals.

The model showed increased terminal embolization occurred with decrease in embolus deposition rate, increase in embolus diameter and increase in embolus introduction rate. Interestingly, due to the MCA's more expansive structure it was found, for a higher embolus deposition rate, the MCA was less prone to occlusion and focal ischemia than the ACA. However, for a lower embolus deposition rate they both had identical embolization dynamics.

The results can help us in our understanding of the dynamics of embolus transport including that the embolus diameter was important when comparing blockages in different vascular territories, and that asymmetric vasculature is expected to have less blockages compared to simplified symmetric vasculature. The activation of autoregulation in the model was only seen to marginally reduce the vascular blockage from emboli.

In future, we can couple this branching tree fractal model with 3D patient-specific CFD model of the CoW to see the trajectory and distribution of emboli through this system.

References

[1] Russell, D., Cerebral microemboli and cognitive impairment. *J Neurol Sci,* **203-204**, pp. 211-214, 2002.

[2] Purandare, N., Burns, A., Daly, K.J., Hardicre, J., Morris, J., Macfarlane, G. & McCollum, C., Cerebral emboli as a potential cause of Alzheimer's

disease and vascular dementia: Case-control study. *Brit Med J,* **332**, pp. 1119-1124, 2006.
[3] Vermeer, S., Jr, W.L. & Koudstaal, P., Silent brain infarcts: a systematic Review. *Lancet Neurol,* **6,** pp. 611-619, 2007.
[4] Hossmann, K.A., Cerebral ischemia: models, methods and outcomes. *Neuropharmacology*, **55**, pp. 257-270, 2008.
[5] Atochin, D., Murciano, J., Gürsoy-Özdemir, Y., Kraisik, T., Noda, F., Ayata, C., Dunn, A., Moskowitz, M., Huang, P. & Muzykantov, V., Mouse model of microembolic stroke and reperfusion. *Stroke*, **35**, pp. 2177-2182, 2004.
[6] Niimi, H., Komai, Y., Yamaguchi, S. & Seki, J., Microembolic flow disturbances in the cerebral microvasculature with an arcadal network: A numerical simulation. *Clin Hemorheol Micro,* **34**, pp. 247-255. 2006.
[7] Chung E.M.L., Hague, J.P. & Evans, D.H., Revealing the mechanisms underlying embolic stroke using computational modelling. *Phys Med Biol* **52**, pp. 7153-7166, 2007.
[8] Hague J.P. & Chung E.M.L., Statistical physics of cerebral embolization leading to stroke. *Physical Review E*, **80(5)** Article Number: 051912, Part 1, pp. 051912-1-051912-9, 2009.
[9] Hudetz, A., Jr, J.H., Horton, C., Conger, K. & Reneau, D., Mathematical simulation of cerebral blood flow in focal ischemia. *Stroke*, **13**, pp. 693-700, 1982.
[10] Bagchi, P., Mesoscale simulation of blood flow in small vessels. *Biophys J*, **92**, pp. 1858-1877, 2007.
[11] AlMomani, T., Udaykumar, H.S., Marshall, J.S. & Chandran, K.B., Micro-scale dynamics simulation of erythrocyte-platelet interaction in blood flow. *Ann Biol Eng*, **36**, pp. 905-920, 2008.
[12] Bui, A., Šutalo, I.D., Manasseh, R. & Liffman, K., Dynamics of pulsatile flow in fractal models of vascular branching networks. *Med Biol Eng Comput*, **47**, pp. 763-772, 2009.
[13] Cassot, F., Lauwers, F., Fouard, C., Prohaska, S. & Lawers-Cances, V., A novel three-dimensional computer assisted method for a quantitative study of microvascular networks of the human cerebral cortex. *Microcirculation*, **13**, pp. 1-18, 2006.
[14] Lauwers, F., Cassot, F., Lauwers-Cances, V., Puwanarajah, P. & Duvernoy, H., Morphometry of the human cerebral cortex microcirculation: General characteristics and space-related profiles. *NeuroImage*, **39**, 936-948, 2008.
[15] Schmid-Schönbein G.W., Biomechanics of microcirculatory blood perfusion, *Annu Rev Biomed Eng*, **1**, pp. 73-102, 1999.
[16] Moser, K.M., Guisan, M., Bartimmo, E.E., Longo, A.M., Harsanyi, P.G. & Chiorazzi, N., In vivo and post mortem dissolution rates of pulmonary emboli and venus thrombi in the dog. *Circulatio*n, **48**, pp. 170-178, 1973.
[17] Alevriadou, B. & McIntire, L., Rheology (Chapter 20). *Thrombosis and Hemorrhage,* Blackwell Sci Publ, Boston, pp. 369-381, 1994.
[18] Pollanen, M., Behaviour of suspended particles at bifurcations: implications for embolism. *Phys Med Biol*, **36**, pp. 397-401, 1991.

[19] Bateman, G.A., Levi, C.R., Schofield, P., Wang, Y. & Lovett, E.C., Quantitative measurement of cerebral haemodynamics in early vascular dementia and Alzheimer's disease. *J Clin Neurosci*, **13**, pp. 563-568, 2006.
[20] Niwa, K., Porter, V., Kazama, K., Cornfield, D., Carlson, G. & Iadecola, C., Aβ-peptides enhance vasoconstriction in cerebral circulation, *Am J Physiol Heart Circ Physiol*, **281**, pp. H2417-H2424, 2001.
[21] Schreiner, W., Karch, R., Neumann, M., Neumann, F., Szawlowski, P. & Roedler, S., Optimized arterial trees supplying hollow organs, *Med Eng Phys*, **28**, pp. 416-429, 2006.
[22] Pries, A., Secomb, T. & Gaehtgens, P., Review - Biophysical aspects of blood flow in the microvasculature, *Cardiovasc Res*, **32**, pp. 654-667, 1996.
[23] Davis, T., Alzaidi, S., Chatelin, R. & Farr, H., Coupled autoregulation models, in: IFMBE Proceedings - ICBME 2008, Springer, pp. 1896-1899, 2008.
[24] Girouard, H. & Iadecola, C., Neurovascular coupling in the normal brain and in hypertension, stroke, and Alzheimer disease. Journal of Applied Physiology, **100**, pp. 328-335, 2006.
[25] Vadapalli, A., Goldman, D. & Popel, A., Calculations of oxygen transport by red blood cells and hemoglobin solutions in capillaries, *Artif Cell Blood Sub*, **30(3)**, pp. 157-188, 2002.
[26] Kavanagh, B., Secomb, T., Hsu, R., Lin, P., Venitz, J. & Dewhirst, M., A theoretical model for the effects of reduced Hemoglobin-Oxygen affinity on tumor oxygenation. *Int J Radiat Oncol,* **53**, pp. 172-179, 2002.
[27] Boas, D.A., Jones, S.R., Devor, A., Huppert, T.J. & Dale, A.M. A vascular anatomical network model of the spatio-temporal response to brain activation. *NeuroImage*, **40**, pp. 1116-1129, 2008.
[28] Pries, A.R., Leg, K., Claassen, M. & Gaehtgens, P., Red cell distribution at microvascular bifurcations, *Microvasc Res*, **38**, pp. 81-101, 1989.
[29] Goodman, P., Barlow, E., Crapo, P., Mohammad, S., Solen, K., Computational model of device-induced thrombosis and thromboembolism, *Ann Biomed Eng*, **33**, pp. 780-797, 2005.
[30] Wijman, C.A.C., Babikian, V.L., Winter, M.R. & Pochay, V.E., Distribution of cerebral microembolism in the anterior and middle cerebral arteries. *Acta Neurol Scand*, **101**, pp. 122-127,2000.
[31] Šutalo, I.D., Bui, A., Ahmed, S., Liffman, K. & Manasseh, R., Modelling of flow through the circle of Willis and cerebral vasculature, *Modelling in Medicine and Biology VIII,* WIT Transactions on Biomedicine and Health, Vol. 13., *BioMED 2009*, Crete, Greece, pp. 83-92, 2009.
[32] Bui, A.V., Manasseh, R., Liffman, K. & Šutalo, I.D., Development of optimized vascular fractal tree models using level set distance function. *Medical Engineering and Physics*, **32**, pp. 790-794, 2010.
[33] Chung, E.M.L., Hague, J.P., Chanrion, M.A., Ramnarine, K.V., Katsogridakis, E. & Evans, D.H., Embolus trajectory through a physical replica of the major cerebral arteries. *Stroke*, **41(4)**, pp. 647-652, 2010.